future to provide invaluable information for climate and oceanographic research.

See also

Air–Sea Gas Exchange. Carbon Dioxide (CO_2) Cycle. Coral Reef and other Tropical Fisheries. Current Systems in the Indian Ocean. Current Systems in the Southern Ocean. Dispersion in Shallow Seas. Electrical Properties of Sea Water. El Niño Southern Oscillation (ENSO). Evaporation and Humidity. Heat and Momentum Fluxes at the Sea Surface. IR Radiometers. Ocean Circulation. Ocean Color from Satellites. Penetrating Shortwave Radiation. Radiative Transfer in the Ocean. Satellite Altimetry. Satellite Measurements of Salinity. Satellite Oceanography, History and Introductory Concepts. Satellite Remote Sensing SAR. Shelf-sea and Slope Fronts. Thermohaline Circulation. Upper Ocean Time and Space Variability.

Further Reading

Barton IJ (1995) Satellite-derived sea surface temperatures: Current status. *Journal of Geophysical Research* 100: 8777–8790.

Gurney RJ, Foster JL and Parkinson CL (eds) (1993) *Atlas of Satellite Observations Related to Global Change*. Cambridge: Cambridge University Press.

Ikeda M and Dobson FW (1995) *Oceanographic Applications of Remote Sensing*. London: CRC Press.

Kearns EJ, Hanafin JA, Evans RH, Minnett PJ and Brown OB (2000) An independent assessment of Pathfinder AVHRR sea surface temperature accuracy using the Marine-Atmosphere Emitted Radiance Interferometer (M-AERI). Bulletin of the American Meteorological Society. 81: 1525–1536.

Kidder SQ and Vonder Haar TH (1995) *Satellite Meteorology: An Introduction*. London: Academic Press.

Legeckis R and Zhu T (1997) Sea surface temperature from the GEOS-8 geostationary satellite. *Bulletin of the American Meteorological Society* 78: 1971–1983.

May DA, Parmeter MM, Olszewski DS and Mckenzie BD (1998) Operational processing of satellite sea surface temperature retrievals at the Naval Oceanographic Office. *Bulletin of the American Meteorological Society*, 79: 397–407.

Robinson IS (1985) *Satellite Oceanography: An Introduction for Oceanographers and Remote-sensing Scientists*. Chichester: Ellis Horwood.

Stewart RH (1985) *Methods of Satellite Oceanography*. Berkeley, CA: University of California Press.

Victorov S (1996) *Regional Satellite Oceanography*. London: Taylor and Francis.

SATELLITE REMOTE SENSING SAR

A. K. Liu and S. Y. Wu, NASA Goddard Space Flight Center, Greenbelt, MD, USA

doi:10.1006/rwos.2001.0339

Introduction

Synthetic aperture radar (SAR) is a side-looking imaging radar usually operating on either an aircraft or a spacecraft. The radar transmits a series of short, coherent pulses to the ground producing a footprint whose size is inversely proportional to the antenna size, its aperture. Because the antenna size is generally small, the footprint is large and any particular target is illuminated by several hundred radar pulses. Intensive signal processing involving the detection of small Doppler shifts in the reflected signals from targets to the moving radar produces a high resolution image that is equivalent to one that would have been collected by a radar with a much larger aperture. The resulting larger aperture is the 'synthetic aperture' and is equal to the distance traveled by the spacecraft while the radar antenna is collecting information about the target. SAR techniques depend on precise determination of the relative position and velocity of the radar with respect to the target, and on how well the return signal is processed.

SAR instruments transmit radar signals, thus providing their own illumination, and then measure the strength and phase of the signals scattered back to the instrument. Radar waves have much longer wavelengths compared with light, allowing them to penetrate clouds with little distortion. In effect, radar's longer wavelengths average the properties of air with the properties and shapes of many individual water droplets, and are only affected while entering and exiting the cloud. Therefore, microwave radar can 'see' through clouds.

SAR images of the ocean surface are used to detect a variety of ocean features, such as refracting surface gravity waves, oceanic internal waves, wind fields, oceanic fronts, coastal eddies, and intense low pressure systems (i.e. hurricanes and polar lows), since they all influence the short wind waves responsible for radar backscatter. In addition, SAR is the only sensor that provides measurements of the

directional wave spectrum from space. Reliable coastal wind vectors may be estimated from calibrated SAR images using the radar cross-section. The ability of a SAR to provide valuable information on the type, condition, and motion of the sea ice and surface signatures of swells, wind fronts, and eddies near the ice edge has also been amply demonstrated.

With all-weather, day/night imaging capability, SAR penetrates clouds, smoke, haze, and darkness to acquire high quality images of the Earth's surface. This makes SAR the frequent sensor of choice for cloudy coastal regions. Space agencies from the USA, Canada, and Europe use SAR imagery on an operational basis for sea ice monitoring, and for the detection of icebergs, ships, and oil spills. However, there can be considerable ambiguity in the interpretation of physical processes responsible for the observed ocean features. Therefore, the SAR imaging mechanisms of ocean features are briefly described here to illustrate how SAR imaging is used operationally in applications such as environmental monitoring, fishery support, and marine surveillance.

History

The first spaceborne SAR was flown on the US satellite Seasat in 1978. Although Seasat only lasted 3 months, analysis of its data confirmed the sensitivity of SAR to the geometry of surface features. On March 31, 1991 the Soviet Union became the next country to operate an earth-orbiting SAR with the launch of Almaz-1. Almaz-1 returned to earth in 1992 after operating for about 18 months. The European Space Agency (ESA) launched its first remote sensing satellite, ERS-1, with a C-band SAR on July 17, 1991. Shortly thereafter, the JERS-1 satellite, developed by the National Space Development Agency of Japan (NASDA), was launched on February 11, 1992 with an L-band SAR. This was followed a few years later by Radarsat-1, the first Canadian remote sensing satellite, launched in November 1995. Radarsat-1 has a ScanSAR mode with a 500 km swath and a 100 m resolution, an innovative variation of the conventional SAR (with a swath of 100 km and a resolution of 25 m). ERS-2 was launched in April 1995 by ESA, and Envisat-1 with an Advanced SAR is underway with a scheduled launch date in July 2001. The Canadian Space Agency (CSA) has Radarsat-2 planned for 2002, and NASDA has Advanced Land Observing Satellite (ALOS) approved for 2003. **Table 1** shows all major ocean-oriented spaceborne SAR missions worldwide from 1978 to 2003.

Table 1 Major ocean-oriented spaceborne SAR missions

Platform	*Nation*	*Launch*	*Band*[a]	*Status*
Seasat	USA	1978	L	Ended
Almaz-1	USSR	1991	S	Ended
ERS-1	Europe	1991	C	Standby
JERS-1	Japan	1992	L	Ended
ERS-2	Europe	1995	C	Operational
Radarsat-1	Canada	1995	C	Operational
Envisat-1	Europe	2001	C	Launch scheduled
Radarsat-2	Canada	2002	C	Approved
ALOS	Japan	2003	L	Approved

[a]Some frequently used radar wavelengths are: 3.1 cm for X-band, 5.66 cm for C-band, 10.0 cm for S-band, and 23.5 cm for L-band.

Aside from these free-flying missions, a number of early spaceborne SAR experiments in the USA were conducted using shuttle imaging radar (SIR) systems flown on NASA's Space Shuttle. The SIR-A and SIR-B experiments, in November 1981 and October 1984, respectively, were designed to study radar system performance and obtain sample data of the land using various incidence angles. The SIR-B experiment provided a unique opportunity for studying ocean wave spectra due to the relatively lower orbit of the Shuttle as compared with satellites. The low orbital altitude increases the frequency range of ocean waves that could be reliably imaged, because blurring of the detected waves caused by the motion of ocean surface during the imaging process is reduced. The final SIR mission, SIR-C in April and October 1994, simultaneously recorded SAR data at three wavelengths (L-, C-, and X-bands). These multiple-frequency data from SIR-C improved our understanding of the radar scattering properties of the ocean surface.

Imaging Mechanism of Ocean Features

For a radar with an incidence angle of 20°–50°, such as all spaceborne SARs, backscatter from the ocean surface is produced primarily by the Bragg resonant scattering mechanism. That is, surface waves traveling in the radar range (across-track) direction with a wavelength of $\lambda/(2\sin\theta)$, called the Bragg resonant waves, account for most of the backscattering. In this formula, λ is the radar wavelength, and θ is the incidence angle. In general, the Bragg resonant waves are short gravity waves with wavelengths in the range of 3–30 cm, depending on the radar wavelength or band, as shown in **Table 1**. Because SAR is most sensitive to waves of this wavelength, or roughness of this scale, any

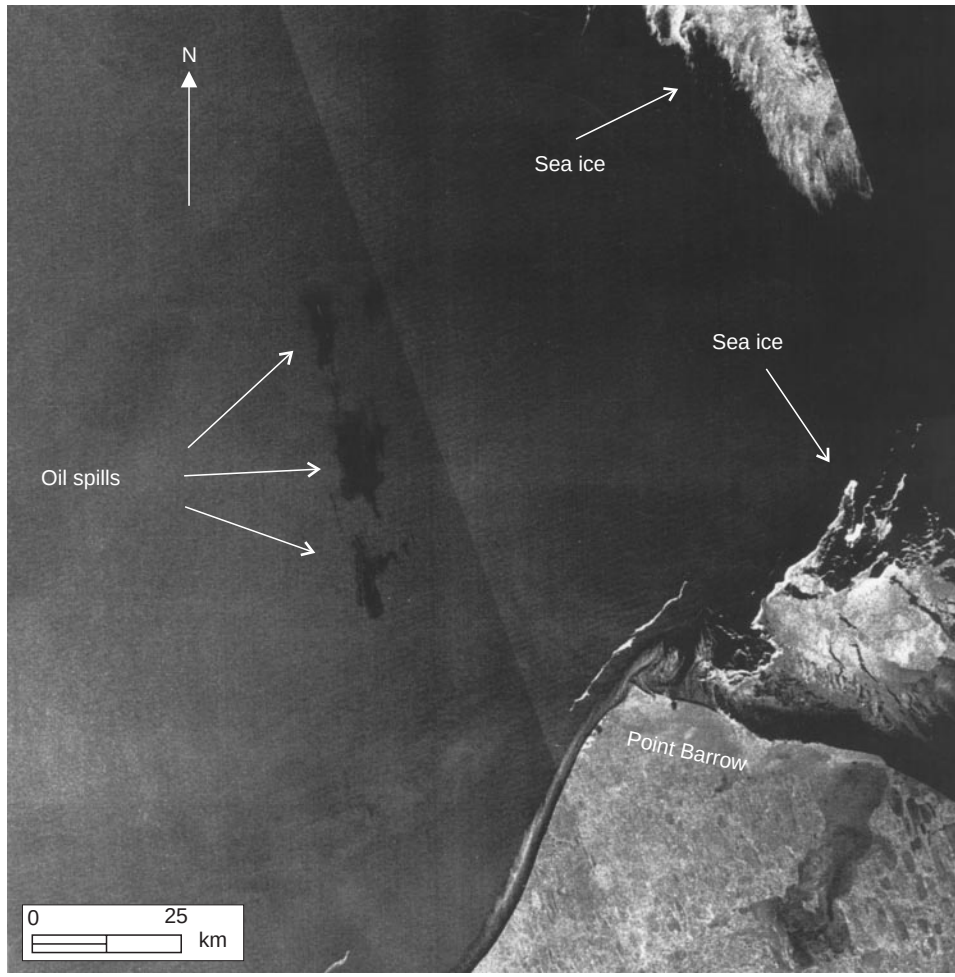

Figure 1 Radarsat ScanSAR image of oil spills off Point Barrow, Alaska, collected on November 2, 1997. (© CSA 1997.)

ocean phenomenon or process that produces modulation in these particular wavelengths is theoretically detectable by SAR. The radar cross-section of the ocean surface is affected by any geophysical variable, such as wind stress, current shear, or surface slicks, that can modulate the ocean surface roughness at Bragg-scattering scales. Thus, SARs have proven to be an excellent means of mapping ocean features.

For ocean current features, the essential element of the surface manifestation is the interaction between the current field and the wind-driven ocean surface waves. The effect of the surface current is to alter the short-wave spectrum from its equilibrium value, while the natural processes of wave energy input from the wind restores the ambient equilibrium spectrum. A linear SAR system is one for which the variation of the SAR image intensity is proportional to the gradient of the surface velocity. The proportionality depends on radar wavelength, radar incidence angle, angle between the radar look direction and the current direction, azimuth angle, and the wind velocity. Under high wind condition, large wind waves may overwhelm the weaker current feature. When current flows in the cross-wind direction, the wave–current interaction is relatively weak, causing a weak radar backscattering signal.

For ocean frontal features, the change in surface brightness across a front in a SAR image is caused by the change in wind stress exerted onto the ocean surface. The wind stress in turn depends on wind speed and direction, air–sea temperature difference, and surface contamination. The effects of wind stress upon surface ripples and therefore upon radar cross-section, have been modeled and demonstrated as shown in the example below. In the high wind stress area, the ocean surface is rougher and appears as a brighter area in a SAR image. On the other side of the front where the wind is lower, the surface is smoother and appears as a darker area in a SAR image.

The reason why surface films are detectable on radar images is that oil films have a dampening effect on short surface waves. Radar is remarkably

Figure 2 ERS-1 SAR image of shallow water bathymetry at Taiwan Tan acquired on July 27, 1994. (© ESA 1994.)

sensitive to small changes in the roughness of sea surface. Oil slicks also have a dark appearance in radar images and are thus similar to the appearance of areas of low winds. The distinctive shape and sharp boundary of localized surface films allows them to be distinguished from the relatively large regions of low wind.

Examples of Ocean Features from SAR Applications

A number of important SAR applications have emerged recently, particularly since ERS-1/2, and Radarsat-1 data became available and the ability to process SAR data has improved. In the USA, the National Oceanic and Atmospheric Administration (NOAA) and the National Ice Center use SAR imagery on an operational basis for sea ice monitoring, iceberg detection, fishing enforcement, oil spill detection, wind and storm information. In Canada, sea ice surveillance is now a proven near-real-time operation, and new marine and coastal applications for SAR imagery are still emerging. In Europe, research on SAR imaging of ocean waves has received great attention in the past 10 years, and has contributed to better global ocean wave forecasts. However, the role of SAR in the coastal observing system still remains at the research and development stage. For reference, examples of some typical ocean features from SAR applications are provided below.

For marine environmental monitoring, features such as oil spills, bathymetry, and polar lows are important for tracking and can often be identified easily with SAR. In early November 1997,

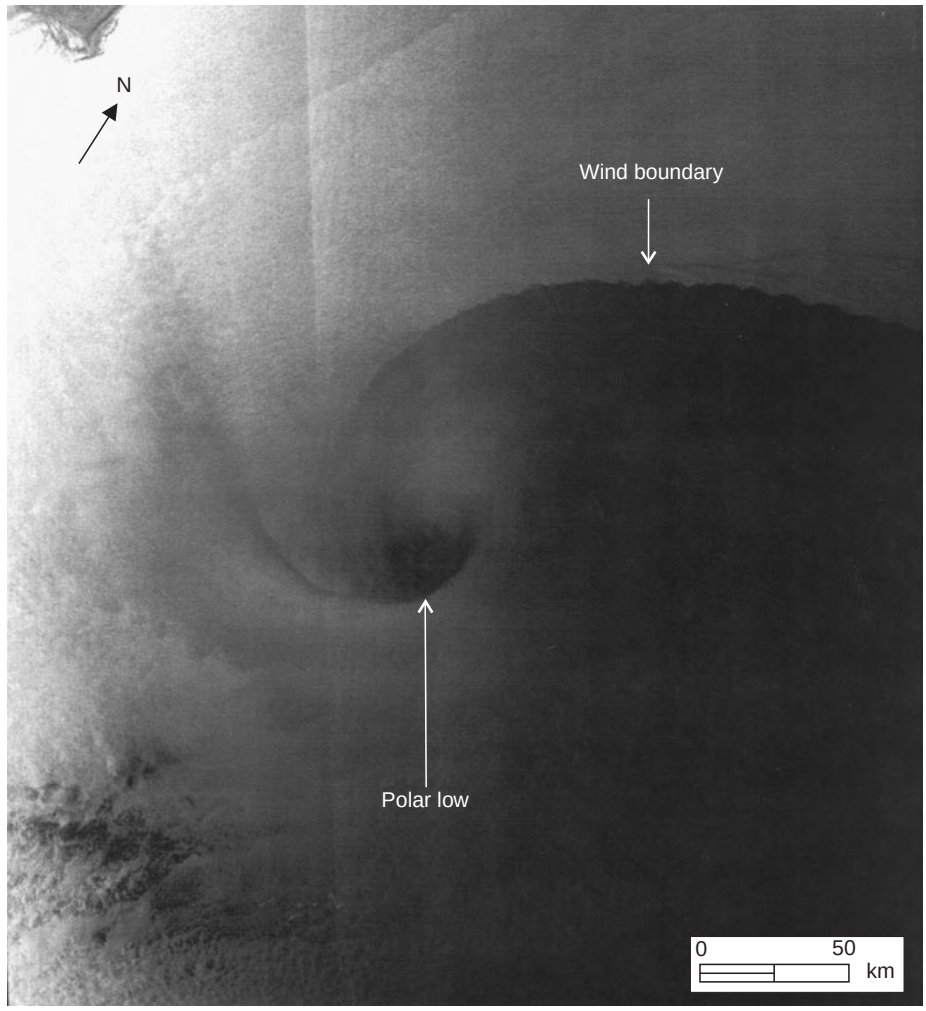

Figure 3 Radarsat ScanSAR image of a polar low in the Bering Sea collected on February 5, 1998. (© CSA 1998.)

Radarsat's SAR sensor captured an oil spill off Point Barrow, Alaska. The oil slicks showed up clearly on the ScanSAR imagery on November 2, 3 and 9. The oil spill is suspected to be associated with the Alaskan Oil Pipeline. **Figure 1** shows a scene containing the oil slicks cropped out from the original ScanSAR image for a closer look. Tracking oil spills using SAR is useful for planning clean-up activities. Early detection, monitoring, containment, and clean up of oil spills are crucial to the protection of the environment.

Under favorable wind conditions with strong tidal current, the surface signature of bottom topography in shallow water has often been observed in SAR images. **Figure 2**, showing an ERS-1 SAR image of the shallow water bathymetry of Taiwan Tan collected on July 27, 1994, is such an example. Taiwan Tan is located south west of Taiwan in the Taiwan Strait. Typical water depth there is around 30 m with a valley in the middle and the continental shelf break to the south. An extensive sand wave field (**Figure 2**) is developed at Taiwan Tan regularly by wind, tidal current, and surface waves. Monitoring the changes of bathymetry is critical to ship navigation, especially in the areas where water is shallow and ship traffic is heavy.

Intense low pressure systems in polar regions, often referred to as polar lows, may develop above regions between colder ice/land and warmer ocean during cold air outbreaks. These intense polar lows are formed off major jet streams in cold air masses. Since they usually occur near polar regions where data are sparse, SAR images have been a useful tool for studying these phenomena. **Figure 3** shows a Radarsat ScanSAR image of a polar low in the Bering Sea (centered at 58.0°N, 174.9°E) collected on February 5, 1998. It has a wind boundary to the north spiraling all the way to the center of the storm that separates the high wind (bright) area from the low wind (dark) area. The rippled character along

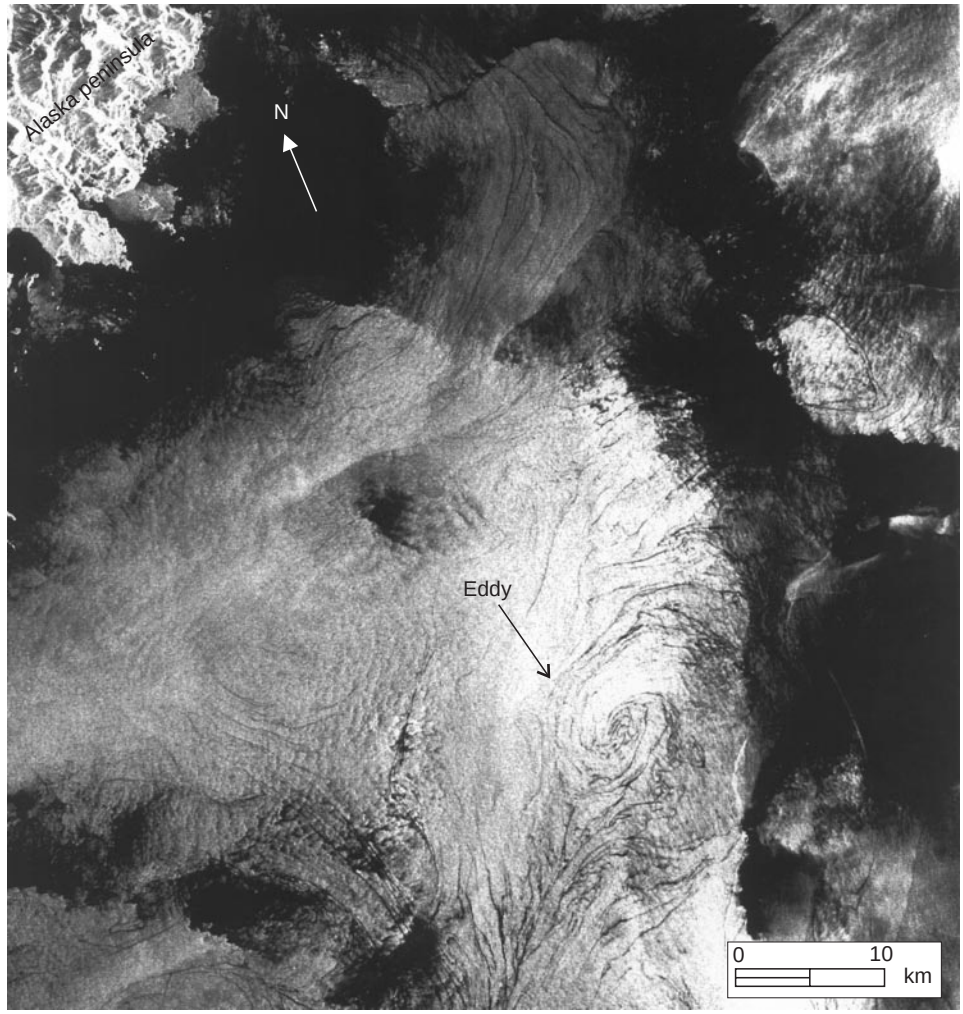

Figure 4 ERS-1 SAR image of lower Shelikof Strait, acquired on October 23, 1991 showing a spiral eddy. (© ESA 1991.)

the wind boundary indicates the presence of an instability disturbance induced by the shear flow, which in turn is caused by the substantial difference in wind speed across the boundary.

Ocean features such as eddies, fronts, and ice edges can result in changes in water temperature, turbulence, or transport and may be the primary determinant of recruitment to fisheries. The survival of larvae is enhanced if they remain on the continental shelf and ultimately recruit to nearshore nursery areas. Features such as fronts and eddies can retain larval patches within the shelf zone. **Figure 4** shows an ERS-1 SAR image acquired on October 23, 1991 (centered at 56.69°N, 156.07°W) in lower Shelikof Strait, the Gulf of Alaska. In this image, an eddy with a diameter of approximately 20 km is visible due to low wind conditions. The eddy is characterized by spiraling curvilinear lines which are most likely associated with current shears, surface films, and to a lesser extent temperature contrasts. SAR has the potential to locate these eddies over extensive areas in coastal oceans.

A Radarsat ScanSAR image over the Gulf of Mexico taken on November 23, 1997 (**Figure 5**) shows a distinct, nearly straight front stretching at least 300 km in length. The center of the front in this scene is in the Gulf of Mexico some 400 km south west of New Orleans. The frontal orientation is about 76° east of north. Closer inspection reveals that there are many surface film-like filaments on the south side of the front. Concurrent wind data suggest that surface currents converge along the front. Therefore, the formation of this front is probably caused by the accumulation of natural surface films brought about by the convergence around the front. This example highlights SAR's sensitivity to the changes of wind speed and the presence of surface films.

The edge of the sea ice has been found to be highly productive for plankton spring bloom and

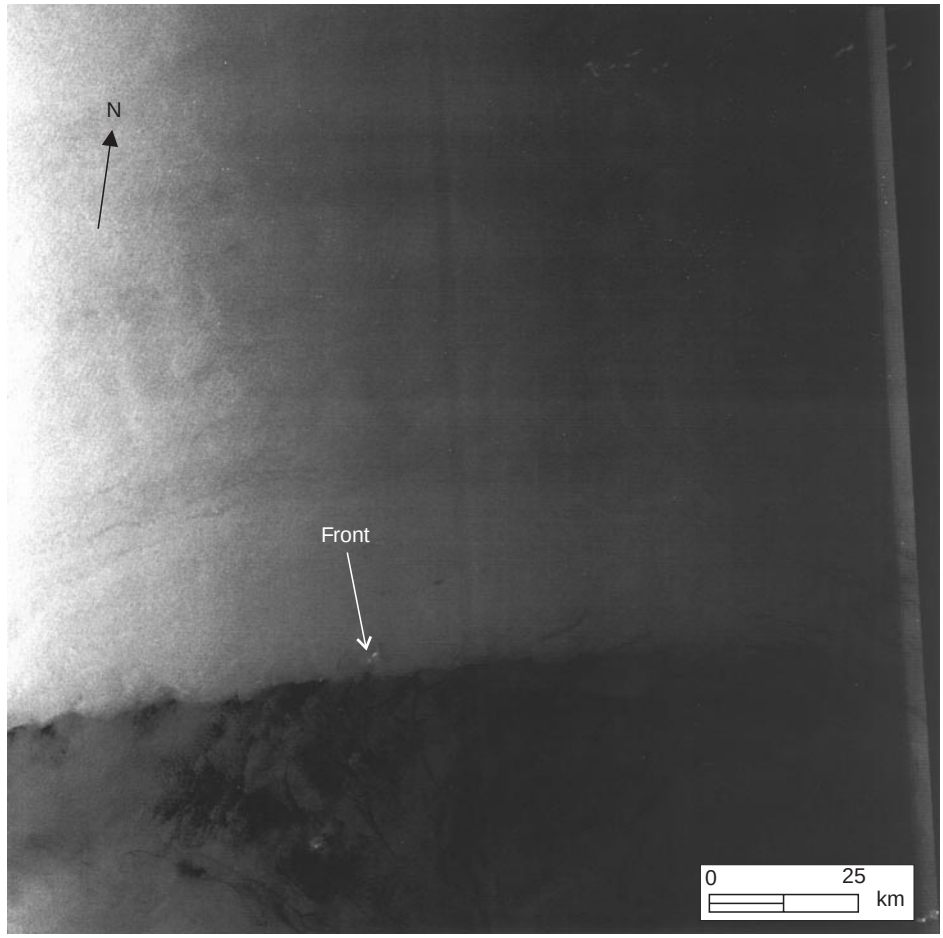

Figure 5 Radarsat ScanSAR image collected over the Gulf of Mexico on November 23, 1997 showing a frontal boundary. (© CSA 1997.)

fishery feeding. In the Bering Sea, fish abundance is highly correlated with yearly ice extent because for their survival many species of fish prefer the cold pools left behind after ice retreat. SAR images are very useful for tracking the movement of the ice edge. **Figure 6** shows a Radarsat ScanSAR image near the ice edge in the Bering Sea collected on February 29, 2000 (centered at 59.6°N and 177.3°W). The sea ice pack with ice bands extending from the ice edge can be clearly seen as the bright area because sea ice surface is rougher than ocean surface (dark area). In the same image, a front is also visible and may or may not be associated with the ice edge to the north. The cold water near the ice edge dampens wave action and appears as a darker area compared with the other side of the front, where it shows up as brighter area due to higher wind and higher sea states.

Information on surface and internal waves, as well as ship wakes, are very important and valuable for marine surveillance and ship navigation. The principal use of SAR for oceanographic studies has been for the detection of ocean waves. The wave direction and height derived from SAR data can be incorporated into models of wind–wave forecast and other applications such as wave–current interaction. **Figure 7** shows an ERS-1 SAR image of long surface waves (or swells) in the lower Shelikof Strait collected on October 17, 1991 (centered at 56.11°N, 156.36°W). The location is close to that of the spiral eddy shown in **Figure 4**. Because of the higher winds and higher sea states at the time the image was acquired, the eddy is less conspicuous in this SAR image taken 6 days earlier. Although the direct surface signature of the eddy cannot be discerned clearly in this image, the wave refraction in the eddy area can still be observed. The rays of the wave field can be traced out directly from the SAR image. The ray pattern provides information on the wave refraction pattern and on the relative variation of wave energy along a ray through wave–current interaction.

Tidal currents flowing over submarine topographic features such as a sill or continental shelf in

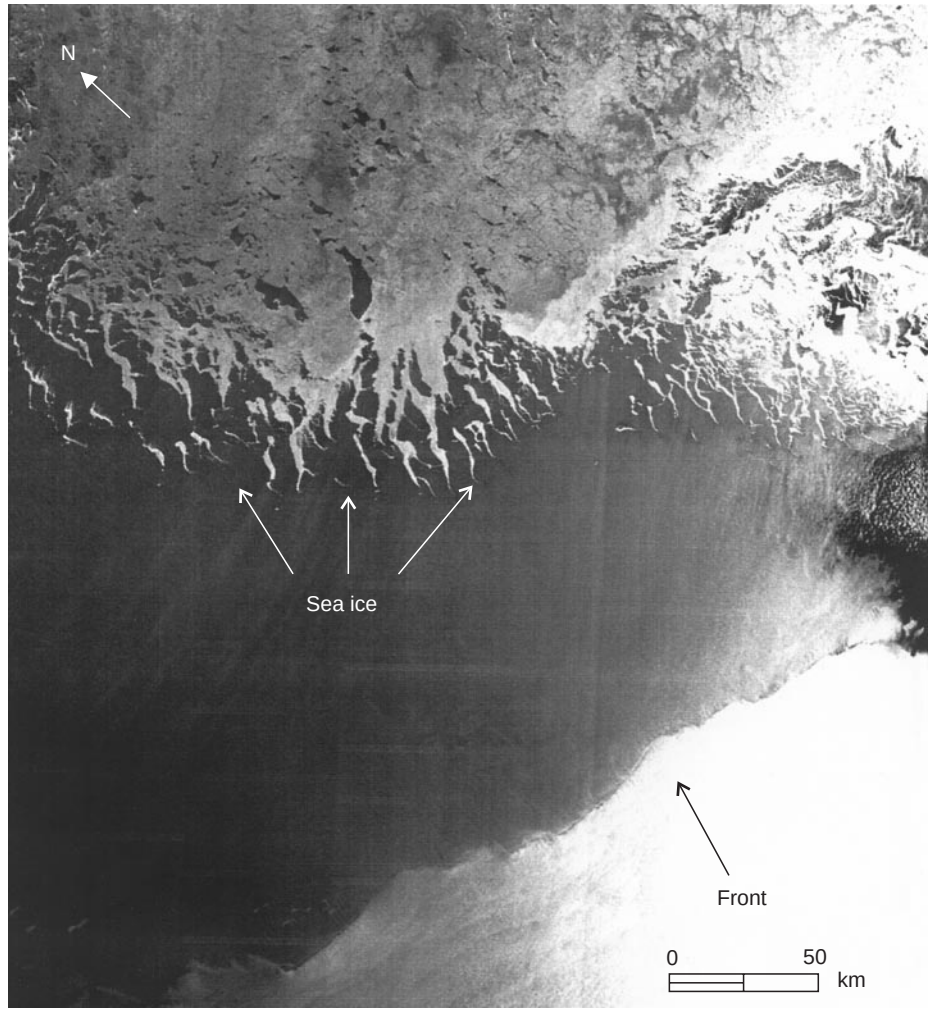

Figure 6 Radarsat ScanSAR image collected over the Bering Sea on February 29, 2000 showing a front near the ice edge. (© CSA 2000.)

a stratified ocean can generate nonlinear internal waves of tidal frequency. This phenomenon has been studied by many investigators. Direct observations have lent valuable insight into the internal wave generation process and explained the role they play in the transfer of energy from tides to ocean mixing. These nonlinear internal waves are apparently generated by internal mixing as tidal currents flow over bottom features and propagate in the open ocean. In the South China Sea near DongSha Island, enormous westward propagating internal waves from the open ocean are often confronted by coral reefs on the continental shelf. As a result, the waves are diffracted upon passing the reefs. **Figure 8** shows a Radarsat ScanSAR image collected over the northern South China Sea on April 26, 1998, showing at least three packets of internal waves. Each packet consists of a series of internal waves, and the pattern of each wave is characterized by a bright band followed immediately by a dark band. The bright/dark bands indicate the contrast in ocean rough/smooth surfaces caused by convergence/divergence areas induced by the internal waves. At times, the wave 'crest' as observed by SAR from the length of bands can be over 200 km long. After passing the DongSha coral reefs, the waves regroup themselves into two separate packets of internal waves. Later, they interact with each other and emerge as a single wave packet again. SAR can be a very useful tool for studying these shelf processes and the effect of the internal waves on oil drilling platforms, nutrient mixing, and sediment transport.

Ships and their wakes are commonly observable in high-resolution satellite SAR imagery. Detection of ships and ship wakes by means of remote sensing can be useful in the areas of national defense intelligence, shipping traffic, and fishing enforcement. **Figure 9** is an ERS-1 SAR image collected on May 31,

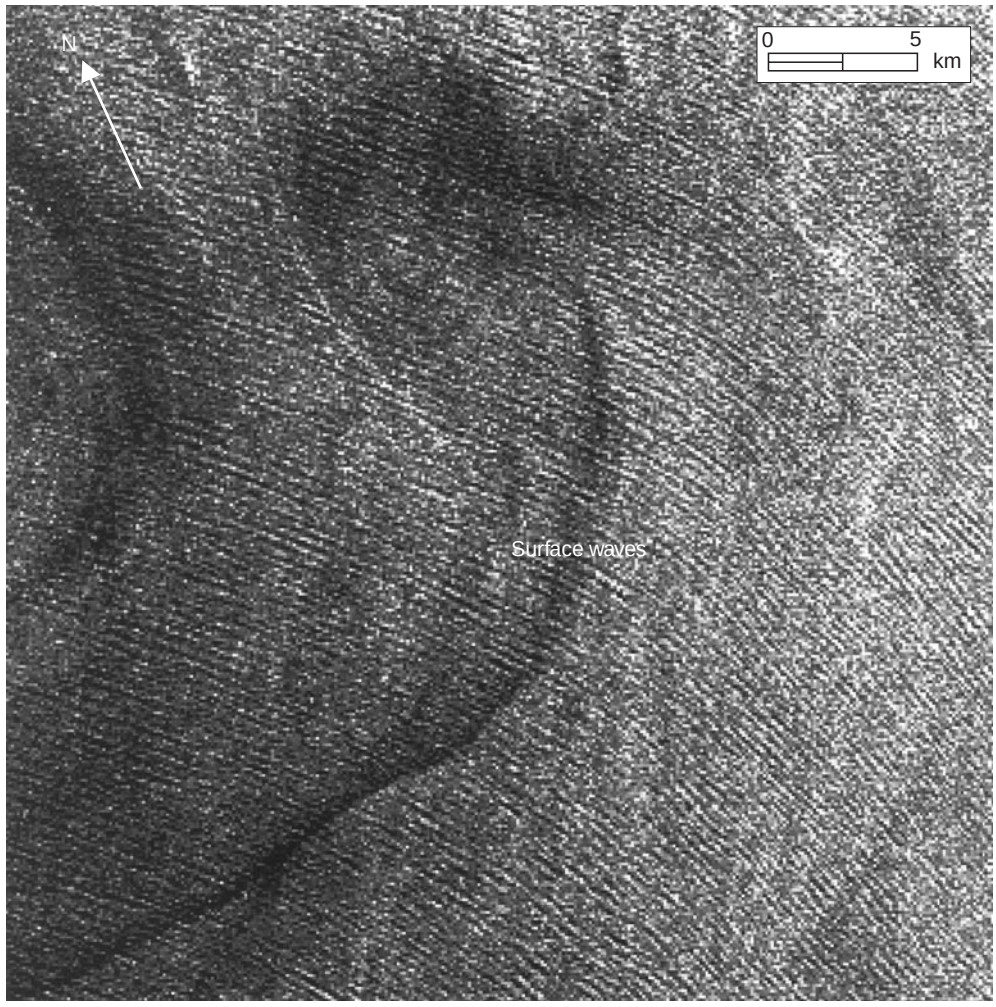

Figure 7 ERS-1 SAR image of lower Shelikof Strait, obtained on October 17, 1991 showing long surface gravity waves refracted by current. (© ESA 1991.)

1995 near the northern coast of Taiwan. The image is centered at 25.62°N and 121.15°E, approximately 30 km offshore in the East China Sea. A surface ship heading north east, represented by a bright spot, can be easily identified. Behind this ship, a long dark turbulence wake is clearly visible. The turbulent wake dampens any short waves, resulting in an area with low backscattering as indicated by the arrow A in **Figure 9**. Near the ship, the dark wake is accompanied by a bright line which may be caused by the vortex shed by the ship into its wake. The ship track follows the busy shipping lane between Hong Kong, Taiwan, and Japan. The ambient dark slicks are natural surface films induced by upwelling on the continental shelf. In the lower part of the image, another ship turbulent wake (long and dark linear feature oriented east–west) can be identified near the location B in **Figure 9**. A faint bright line connects to the end of this turbulent wake, forming a V-shaped wake in the box B. The faintness of this second ship may be caused by very low backscattering of the ship configuration or the wake could have been formed by a submarine. In the latter case, it must have been operating very close to the ocean surface, since the surface wake is observable. The ship wake is pointing to the east, indicating that the faint ship was moving from mainland China toward the open ocean.

Discussion

As mentioned earlier, SAR has the unique capability of operating during the day or night and under all weather conditions. With repeated coverage, spaceborne SAR instruments provide the most efficient means to monitor and study the changes in important elements of the marine environment. As demonstrated by the above examples, the use of SAR-

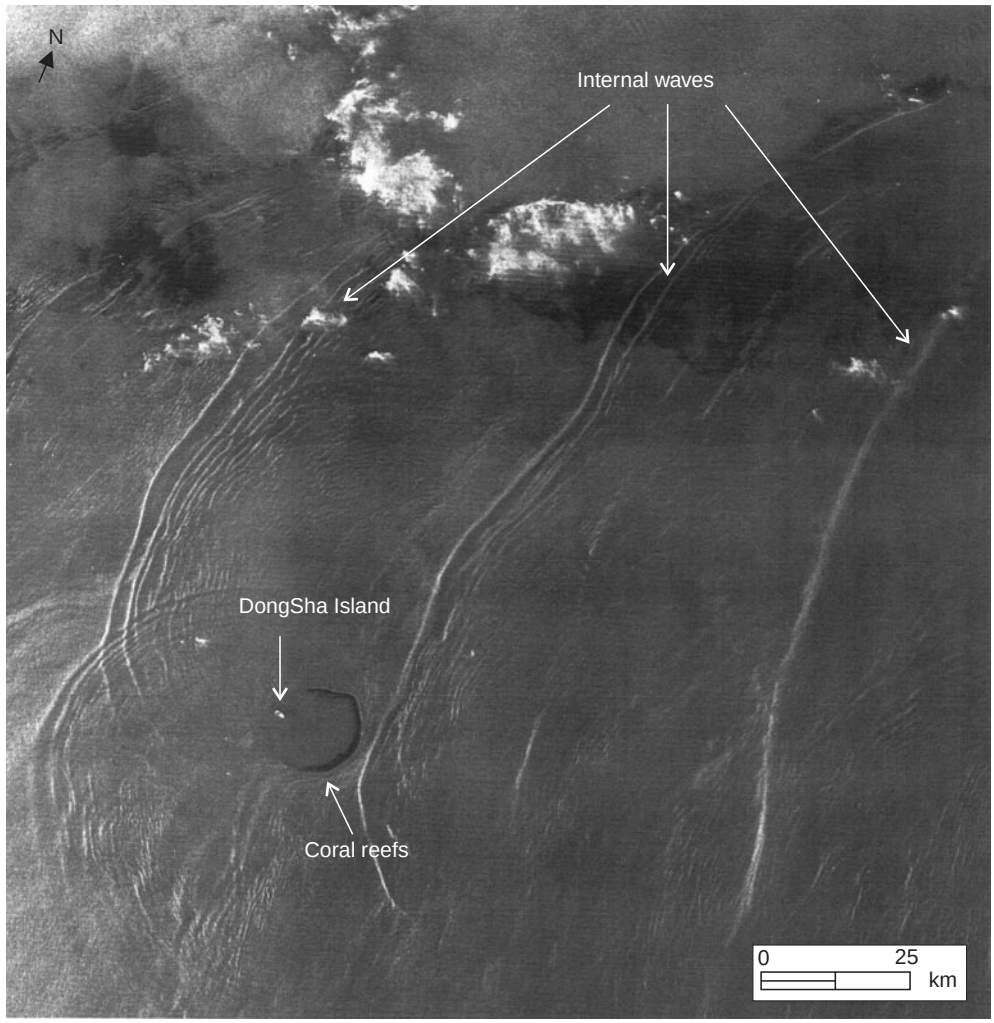

Figure 8 Radarsat ScanSAR image collected over the South China Sea on April 26, 1998 showing three internal wave packets. (© CSA 1998.)

derived observations to track eddies, fronts, ice edges, and oil slicks can supply valuable information and can aid in the management of the fishing industry and the protection of the environment. In overcast coastal areas at high latitudes, the uniformly cold sea surface temperature and persistent cloud cover preclude optical and infrared measurement of surface temperature features, and obscure ocean color observations. The mapping of ocean features by SAR in these challenging coastal regions is, therefore, a potentially major application for satellite-based SAR, particularly for the wider swath ScanSAR mode. Furthermore, SAR data provide unique information for studying the health of the Earth system, as well as critical data for natural hazards and resource assessments.

The prospect of SAR data collection extending well into the twenty-first century gives impetus to current research in SAR applications in ocean science and opens the doors to change detection studies on decadal timescales. The next step is to move into the operational use of SAR data to complement ground measurements. The challenge is to increase cooperation in the scheduling, processing, dissemination, and pricing of SAR data from all SAR satellites between international space agencies. Such cooperation might permit near-real-time high-resolution coastal SAR measurements of sufficient temporal and spatial coverage to impact weather forecasting for selected heavily populated coastal regions. It is necessary to bear in mind that each satellite image is a snapshot and can be complemented with buoy and ship measurements. Ultimately, these data sets should be integrated by numerical models. Such validated and calibrated models will prove extremely useful in understanding a wide variety of oceanic processes.

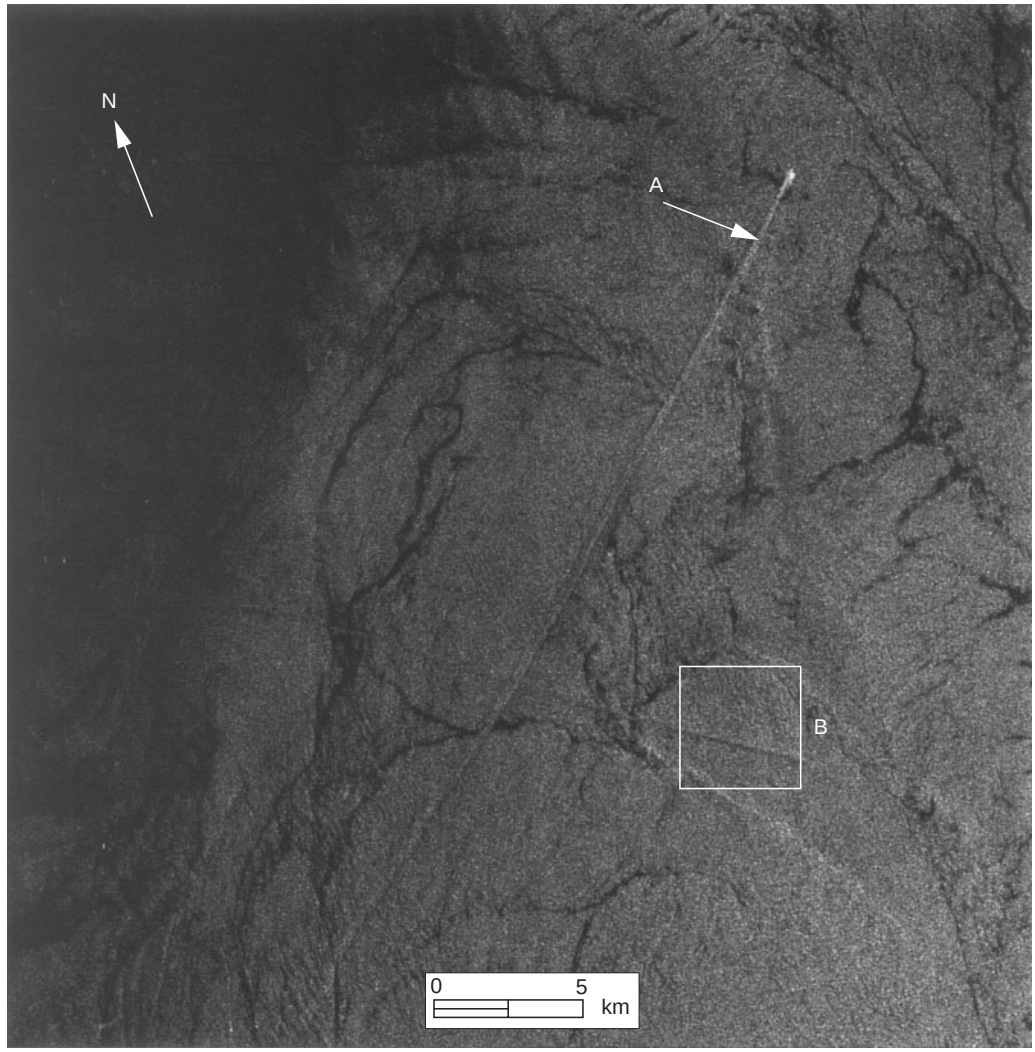

Figure 9 ERS-1 SAR image of East China Sea, obtained on May 31, 1995 showing a surface ship and its wake (arrow A) and a V-shaped wake in box B. (© ESA 1995.)

See also

Aircraft Remote Sensing. Beaches, Physical Processes affecting. Ice–Ocean Interaction. Satellite Altimetry. Satellite Oceanography, History and Introductory Concepts. Satellite Passive Microwave Measurements of Sea Ice. Satellite Remote Sensing Microwave Scatterometers. Satellite Remote Sensing of Sea Surface Temperatures. Surface Films. East Australian Current. Wave Generation by Wind.

Further Reading

Alaska SAR Facility User Working Group (1999) *The Critical Role of SAR in Earth System Science*. (http://www.asf.alaska.edu/)

Beal RC and Pichel WG (eds) (2000) *Coastal and Marine Applications of Wide Swath SAR*. Johns Hopkins APL Technical Digest, 21.

European Space Agency (1995) *Scientific Achievements of ERS-1*. ESA SP-1176/I.

Fu L and Holt B (1982) *Seasat Views Oceans and Sea Ice with Synthetic Aperture Radar*, JPL Publication, pp. 81–120. Pasadena, CA: NASA, JPL/CIT.

Hsu MK, Liu AK and Liu C (2000) An internal wave study in the China Seas and Yellow Sea by SAR. *Continental Shelf Research* 20: 389–410.

Liu AK, Peng CY and Schumacher JD (1994) Wave–current interaction study in the Gulf of Alaska for detection of eddies by SAR. *Journal of Geophysical Research* 99: 10075–10085.

Liu AK, Peng CY and Weingartner TJ (1994) Ocean–ice interaction in the marginal ice zone using SAR. *Journal of Geophysical Research* 99: 22391–22400.

Liu AK, Peng CY and Chang YS (1996) Mystery ship detected in SAR image. *EOS, Transactions, American Geophysical Union* 77: 17–18.

Liu AK, Peng CY and Chang YS (1997) Wavelet analysis of satellite images for coastal watch. *IEEE Journal of Oceanic Engineering* 22: 9–17.

Tsatsoulis C and Kwok R (1998) *Analysis of SAR Data of the Polar Oceans*. Berlin: Springer-Verlag.